Active screen plasma nitriding of 316 stainless steel for the application of bipolar plates in proton exchange membrane fuel cells

Lin, Kaijie; Li, Xiaoying; Sun, Yong; Luo, Xia; Dong, Hanshan

DOI:
10.1016/j.ijhydene.2014.04.102

INTERNATIONAL JOURNAL OF HYDROGEN ENERGY XXX (2014) 1–10

Available online at www.sciencedirect.com

ScienceDirect

journal homepage: www.elsevier.com/locate/he

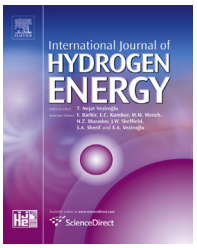

Active screen plasma nitriding of 316 stainless steel for the application of bipolar plates in proton exchange membrane fuel cells

Kaijie Lin [a,*], *Xiaoying Li* [a], *Yong Sun* [b], *Xia Luo* [a], *Hanshan Dong* [a]

[a] *School of Metallurgy and Materials, University of Birmingham, Birmingham B15 2TT, UK*
[b] *Department of Engineering, Faculty of Technology, De Montfort University, Leicester LE1 9BH, UK*

ARTICLE INFO

Article history:
Received 12 October 2013
Received in revised form
27 January 2014
Accepted 12 April 2014
Available online xxx

Keywords:
Bipolar plates
316 Stainless steel
Active screen plasma nitriding
Corrosion resistance
Interfacial contact resistance

ABSTRACT

Proton exchange membrane fuel cell (PEMFC) has attracted considerable interest because of its superb performance, and many researches are focused on the development of high-performance, long-life bipolar plates. Stainless steel bipolar plates offer many advantages over the conventional graphite bipolar plates, such as low material and fabrication cost, excellent mechanical behaviour and ease of mass production. However, the insufficient corrosion resistance and relatively high interfacial contact resistance (ICR) become the major obstacles to the widespread use of stainless steel bipolar plates. In this work, active screen plasma nitriding (ASPN), a novel plasma nitriding technique, was used to modify the surface of 316 austenitic stainless steel. A variety of analytical techniques, including X-ray diffraction (XRD), scanning electron microscopy (SEM), glow discharge optical emission spectrometer (GDOES), were employed to characterize the nitrided samples. The results reveal that a nitrogen supersaturated S-phase layer has been successfully produced on the surface of all nitrided 316 stainless steel samples. The interfacial contact resistance (ICR) value can be decreased dramatically after ASPN treatment and the corrosion resistance can also been improved. In addition, better corrosion resistance can be achieved by active screen plasma nitriding with a stainless steel screen than with a carbon steel screen. This technique could be used to improve the performance and lifespan of bipolar plates for fuel cells.

Introduction

Due to the high power density, nearly zero emission and low operating temperature, proton exchange membrane fuel cell (PEMFC) has been regarded as one of the most promising candidates for transportation and distributed power generation. Bipolar plates, accounting for about 80% of the total weight and 45% of the stack cost [1], are the key multi-functional components in PEMFC stacks, including supporting the membrane electrode assembly, connecting individual cells in stacks, facilitating water and heat management through the cell, and carrying current away from the cell.

* *Corresponding author*. Tel.: +44 (0) 7564157100.
E-mail address: kxl143@bham.ac.uk (K. Lin).

http://dx.doi.org/10.1016/j.ijhydene.2014.04.102

Owing to its good electrical conductivity and corrosion resistance, graphite has been used to fabricate bipolar plates [2]. However, its inherent poor mechanical strength, brittleness and unacceptable high fabrication cost obstruct the wide-spread commercialization of PEMFC [3]. In recent years, more and more researchers pay attention to the application of metals in bipolar plates [4], especially stainless steel, due to its low material cost, relatively high strength and ease of mass production. Nevertheless, the most challenging issues for stainless steel are the insufficient corrosion resistance and poor surface conductivity in aggressive PEMFC working condition, resulting in the power degradation of PEMFC stacks.

To achieve acceptable performance in PEMFC conditions, several surface engineering techniques are employed to address the issues with stainless steel bipolar plates. Many different kinds of coatings, including carbon-based materials [2,5] and metal-based materials [6–8] have been introduced. However, the inherent defects of coatings (such as pinhole) and the high cost, hinder their application.

Wang and Brady [9,10] employed high temperature thermal nitriding to modify the surface properties of 349 austenitic stainless steel. A discontinuous layer, consisting of discrete CrN, Cr_2N and $(Cr, Fe)_2N_{1-x}$ ($x = 0–0.5$), was generated on the surface, which greatly improved the surface conductivity; however, such high-temperature treatment resulted in the degradation of corrosion resistance. Notwithstanding the fact that [11] low-temperature thermal nitriding can provide better corrosion resistance and lower ICR than high temperature thermal nitriding, the corrosion resistance of the low-temperature thermal nitrided samples was not as good as the untreated material as evidenced by the significantly reduced pitting potential. This is mainly because although the treatment temperature (700–900 °C) for so-called 'low-temperature nitriding' was much lower than that of conventional thermal nitriding (1100 °C), precipitation of CrN will occur at temperatures above 500 °C [12], which led to the significant loss of corrosion resistance.

Comparing with thermal nitriding, plasma nitriding can be carried out at temperatures below 500 °C due to sputtering removal of surface passivation film and fast mass transfer. In addition, low temperature (≤450 °C) plasma nitriding can produce a nitrogen supersaturated expanded austenite (or S-phase) layer with combined improvement in hardness and corrosion resistance. This is because plasma nitriding at low-temperature is a paraequilibrium process; whilst small interstitial nitrogen atoms are still mobile, large substitutional chromium atoms cannot move a large enough distance to form CrN precipitates [13]. For example, Tian et al. found that low temperature plasma nitriding slightly improved the corrosion resistance of austenitic stainless steel 316L [14] and 304L [15] in simulated PEMFC environment. Moreover, an improvement in surface conductivity was also found after plasma nitriding. The improvement of corrosion resistance and surface conductivity of stainless steel after low temperature nitriding was also reported by other researchers [16,17].

It should be pointed out that accurate control of temperature is the key to form a S-phase surface layer with enhanced corrosion resistance on stainless steel. However, there are some technical limitations of conventional DC plasma nitriding, such as edge effect, hollow-cathode effect, surface damages and un-uniform nitrided layer. It has been reported recently that severely impaired corrosion resistance at the edge of low-temperature DC plasma nitride components was observed in service mainly due to the local high temperature at edges due to the inherent edge effect of DC plasma [18]. This would become a major concern for DC plasma nitriding of stainless steel bipolar plates because of the large amount of edges of flow channels on the surface of bipolar plates; the precipitation of Cr in those edge areas would lead to serious degradation of corrosion resistance. Moreover, hollow-cathode effect would greatly limit the efficiency of mass production, because specimens cannot be placed close to each other. Those inherent problems make conventional DC plasma nitriding unsuitable for practical application to stainless steel bipolar plates.

A novel surface plasma nitriding technique, active screen plasma nitriding (ASPN), was developed in the late 1990s based on the glow discharge plasma and the principle of post-discharge plasma [19], and it has been extensively studied by many researchers in the past decade [20–22].

Fig. 1 shows the schematic diagrams of DC plasma nitriding (DCPN) and active screen plasma nitriding (ASPN). The essential difference between conventional DC plasma

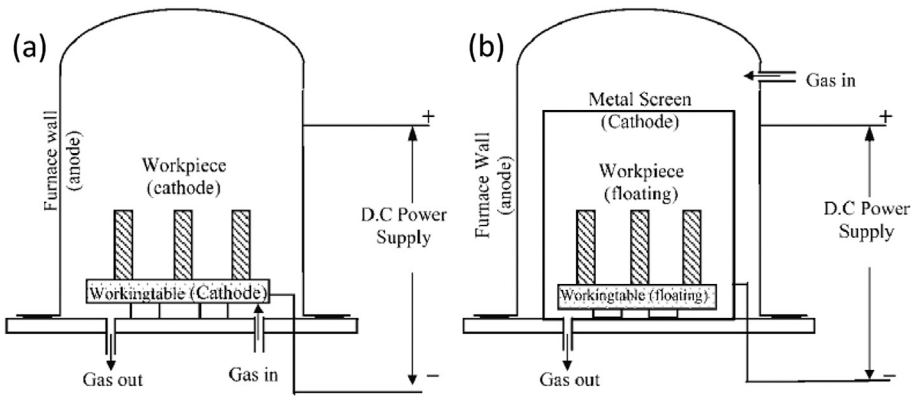

Fig. 1 – Schematic diagrams of conventional direct current plasma nitriding and active screen plasma nitriding. (a) Direct current plasma nitriding (DCPN) (b) Active screen plasma nitriding (ASPN).

Please cite this article in press as: Lin K, et al., Active screen plasma nitriding of 316 stainless steel for the application of bipolar plates in proton exchange membrane fuel cells, International Journal of Hydrogen Energy (2014), http://dx.doi.org/10.1016/j.ijhydene.2014.04.102

Table 1 – The composition of 316 stainless steel.

Element	C	Cr	Mn	Mo	Ni	S	P	Si	Fe
Content (wt%)	0.06	17.20	1.30	2.20	11.70	0.014	0.026	0.60	66.90

nitriding and active screen plasma nitriding is that, the cathodic potential is applied on a metal screen, which surrounds the working table, and the samples to be treated are placed in a floating potential. Under this electrical condition, the plasma can only be formed on the surface of metal screen rather than on the sample surface. Consequently, the active screen plasma nitriding could overcome the inherent limitations of conventional DC plasma nitriding techniques [23], and it possesses the potential for mass production. However, no work has been conducted to study the corrosion behaviour and surface conductivity of low-temperature active-screen plasma nitrided austenitic stainless steel potentially for the bipolar plates in PEMFCs. In this work, the advanced active screen plasma nitriding technique has been used to modify the surface of AISI 316 stainless steel. The corrosion behaviour and surface conductivity of the low-temperature plasma nitrided samples were investigated.

Materials and methods

Commercial austenitic 316 stainless steel was used in this study as the substrate and its chemical composition is shown in Table 1. Coupon samples were cut from hot rolled one inch (25.4 mm) bars and the final dimensions of samples is 25.4 mm in diameter and 6 mm in thickness. The surfaces of samples to be treated were wet ground up to 800# grit using SiC paper. After grinding, samples were washed with soapy water, then ultrasonically cleaned in acetone for 10 min, and finally dried with flowing hot air.

Active screen plasma nitriding experiments were implemented in a AS Plasma Metal 75 kVA industrial scale unit, under a pressure of 0.75 mbar (75Pa) with the gas mixture of 25% N_2 + 75% H_2. Based on our previous work, the treatment temperature was selected as 370 °C, 410 °C, 450 °C for 7 h. This is because when treated at temperatures higher than 450 °C, the corrosion resistance of the plasma treated 316 degraded remarkably due to the precipitation of chromium nitrides [21].

The microstructure and surface morphology of nitrided samples were examined by X-ray diffraction (XRD) and scanning electron microscope (SEM), respectively. Elemental concentration profiles were determined by glow discharge optical emission spectroscopy (GDOES). Surface roughness was measured by Ambios XP-200 stylus profilometer.

Corrosion tests for untreated and the nitrided samples were carried out in a 0.05 M H_2SO_4 solution, which was prepared from analytical grade chemicals and distilled water. All the corrosion tests were conducted at room temperature (20 °C) and in open air condition. The detail of corrosion tests can be found in the literature [24].

Wang's method was used to measure the interfacial contact resistance (ICR) values of samples. The schematic diagram of the method was shown in Fig. 2. Two pieces of carbon paper were sandwiched between the stainless steel sample and copper plates. A constant electrical current was applied via the two copper plates. The compaction force applied on the two copper plates was provided by Zwick universal mechanical tester. By measuring the voltage drop during the increasing of compaction force, it was possible to calculate the total resistance dependency on the compaction force [25].

From Fig. 2, an equation of R_{total} can be obtained (Eq. (1)).

$$R_{total} = 2R_{copper\ plate/carbon\ paper} + R_{carbon\ paper/treated\ side} + R_{carbon\ paper/untreated\ side} + 2R_{copper\ plate} + 2R_{carbon\ paper} + R_{316\ stainless\ steel} \quad (1)$$

To reduce the contact resistance of the untreated side to a negligible value, the untreated side was coated with gold in EMSCOPE SC 500 sputter coater for 3 min. The bulk resistance of stainless steel, copper plate and carbon paper can be neglected. So Eq. (1) can be simplified to Eq. (2).

$$R_{total} = 2R_{copper\ plate/carbon\ paper} + R_{carbon\ paper/treated\ side} \quad (2)$$

A calibration in which only one layer of carbon paper was sandwiched between the two copper plates was employed to correct the interfacial contact resistance between copper plate and carbon paper. Thus, an equation of $R_{calibration}$ can be obtained (Eq. (3)).

$$R_{calibration} = 2R_{copper\ plate/carbon\ paper} \quad (3)$$

The ICR (Eq. (4)) was calculated by subtracting $R_{calibration}$ (Eq. (3)) from R_{total} (Eq. (2)).

$$R_{carbon\ paper/treated\ side} = R_{total} - R_{calibration} \quad (4)$$

All ICR measurements are conducted at room temperature.

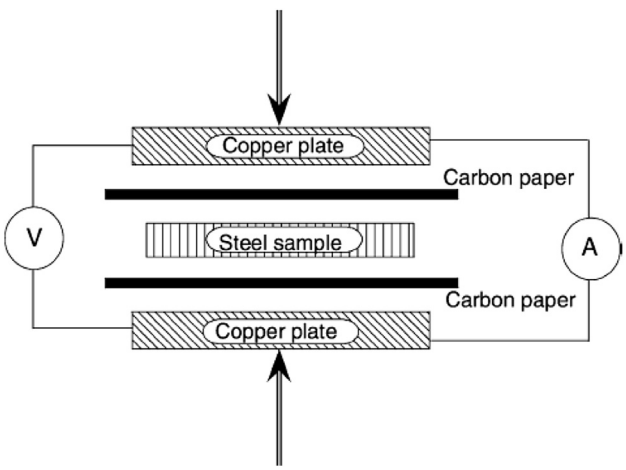

Fig. 2 – Schematic of the test assembly for interfacial contact resistance.

Please cite this article in press as: Lin K, et al., Active screen plasma nitriding of 316 stainless steel for the application of bipolar plates in proton exchange membrane fuel cells, International Journal of Hydrogen Energy (2014), http://dx.doi.org/10.1016/j.ijhydene.2014.04.102

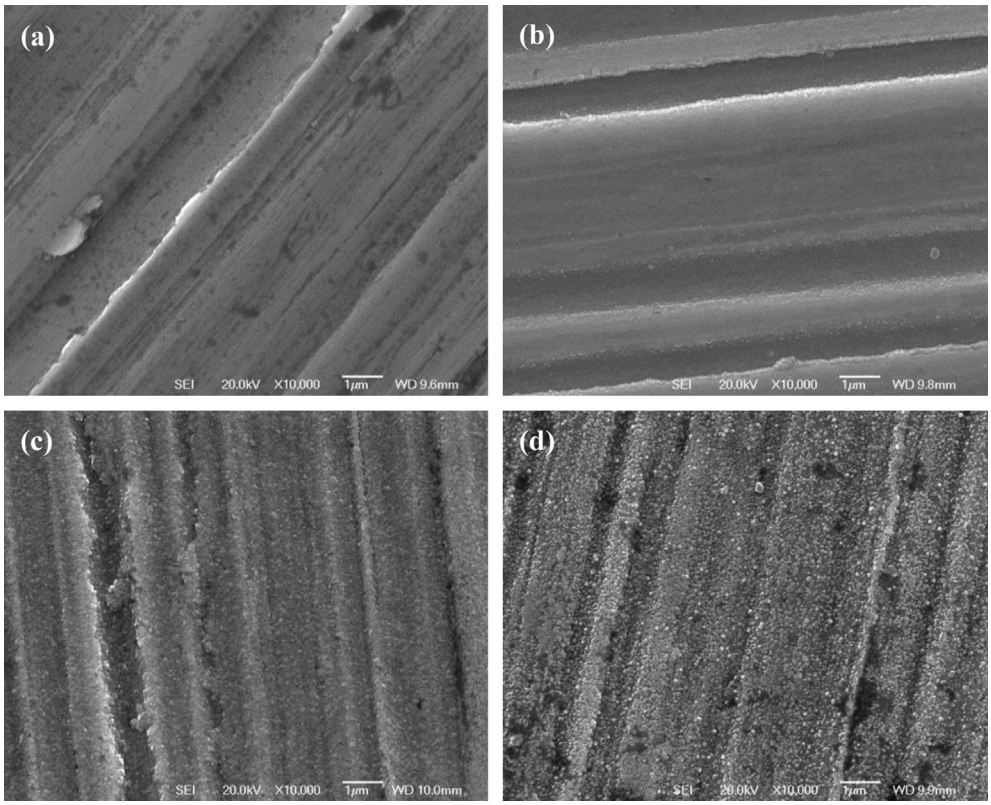

Fig. 3 – SEM images of surface morphologies (a) Before ASPN treatment (b) 370 °C 7 h (c) 410 °C 7 h (d) 450 °C 7 h.

Results and interpretation

Surface morphology and roughness

Fig. 3 shows the surface morphologies of samples before and after ASPN treatment. Because the samples were ground up to 800# grit, the grinding marks are clearly observed from the surface. From Fig. 3(b), it seems that a very thin layer of particles were attached to the surface of 370 °C treated samples, and its surface morphology is almost identical with the untreated one (Fig. 3(a)). With the increase of treatment temperature the surface particle layers became denser and the covered area enlarged. These particles were sputtered from the metal screen and then deposited onto the sample surface during active-screen plasma nitriding [26].

The surface roughness (Ra) of untreated and nitrided samples is summarized in Fig. 4. It can be seen that the surface roughness of 370 °C treated sample is almost identical to that of the untreated one, which confirmed the SEM observations (Fig. 3). Then, the surface roughness increased with the increase of treatment temperature, and a significant rise was observed for 450 °C treated sample.

Microstructure of the nitrided layer

The etchant, 50%HNO_3 + 25% HCl + 25% H_2O, was used to reveal the cross-sectional microstructure of nitrided sample. From Fig. 5, a uniform, featureless and unetched nitrided layer was observed on the surface of each nitrided sample. The thickness of the nitrided layer for 370 °C, 410 °C and 450 °C nitrided sample was 2.0 μm, 3.2 μm and 7.9 μm, respectively. In comparison with the substrate, which suffered from severe localized corrosion, the nitrided layer showed excellent resistance to the attack from corrosive etchant. The bright line between the nitrided layer and the substrate is most probably resulted from the steps formed by mechanical grinding and polishing during sample preparation, because of the huge difference in hardness and thus abrasive wear resistance between the hard surface S-phase layer and the soft austenite substrate [12].

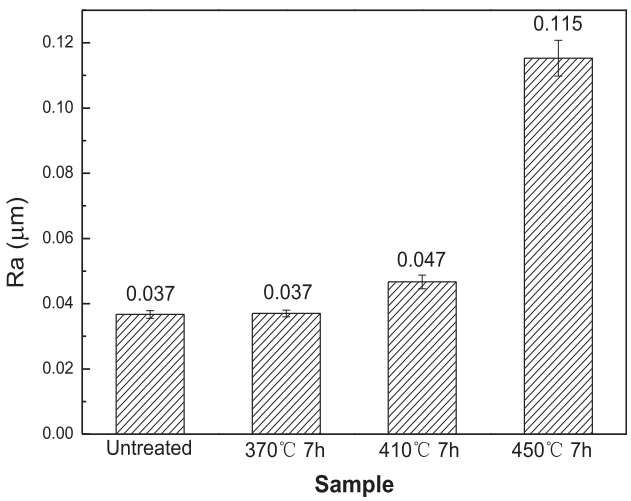

Fig. 4 – Surface roughness of samples.

Please cite this article in press as: Lin K, et al., Active screen plasma nitriding of 316 stainless steel for the application of bipolar plates in proton exchange membrane fuel cells, International Journal of Hydrogen Energy (2014), http://dx.doi.org/10.1016/j.ijhydene.2014.04.102

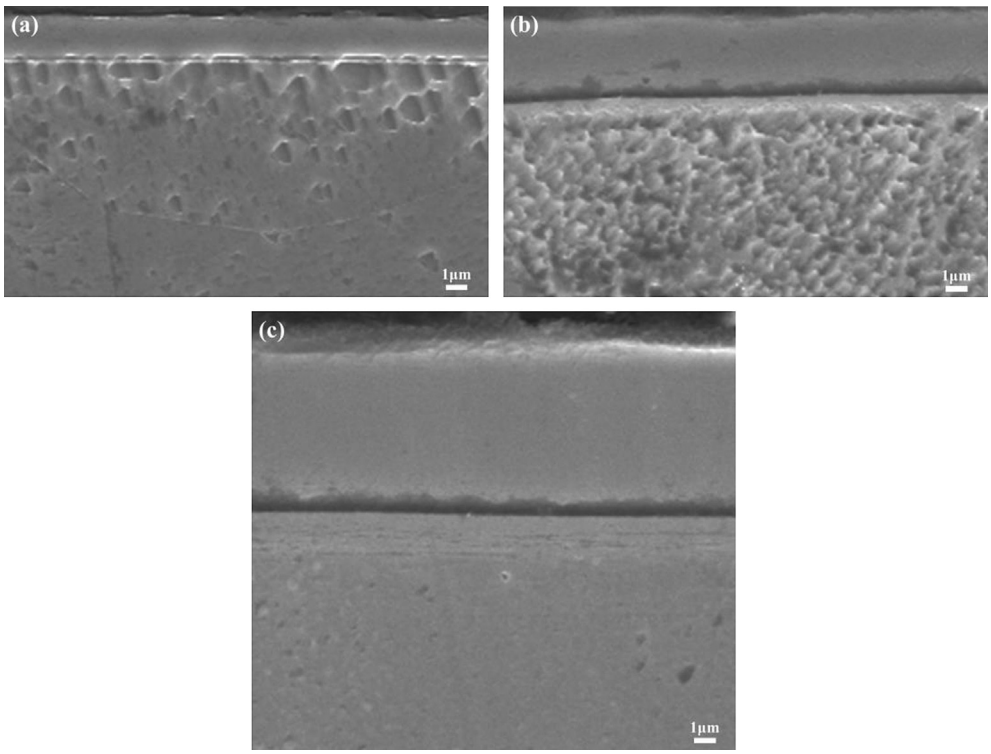

Fig. 5 – Cross-sectional SEM images (a) 370 °C 7 h (b) 410 °C 7 h (c) 450 °C 7 h.

For comparison, direct current plasma nitriding (DCPN) treatment was also conducted at 450 °C for 7 h, with the same gas mixture for ASPN. Fig. 6 shows the cross-sectional back scattered electron SEM images of DCPN treated sample. It can be seen that the nitrided layer formed in the centre area of the DCPNed sample is white (Fig. 6(a)) whilst some dark spots were observed from the edge area (Fig. 6(b)). This implies that precipitation of CrN has most probably occurred at the edge of the DCPN treated sample, which led to the reduced corrosion resistance. Clearly, ASPN has great advantage over DCPN for plasma nitriding of austenitic stainless steel components with corners/edges.

Nitrogen depth-distribution within the nitrided sample was probed by a glow discharge optical emission spectrometer (GDOES). As can be seen from Fig. 7, the nitrogen concentration and depth increased with increasing the treatment temperature, typical for diffusion controlled thermochemical treatment.

Fig. 8 depicts the XRD diffraction patterns of samples before and after ASPN treatments. All nitrided samples produced a new set of peaks, which look similar to that of the untreated material, but shifted to lower angles. These peaks have the characteristics of the nitrogen supersaturated fcc phase, the so-called S-phase [12]. For 370 °C and 410 °C treated samples, because the S-phase layer was thin, X-ray could permeate through it and reach the substrate, the peaks from 316 stainless steel substrate could be detected. It is noted that the extent of angle shifting is different for samples treated at different temperatures, especially for 450 °C treated sample. This is because of the different nitrogen saturation levels and the higher the nitrogen saturation level, the larger d-spacing, and thus the lower angle [27].

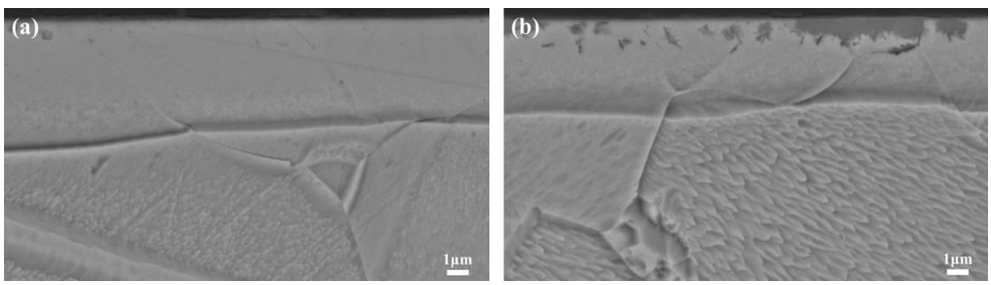

Fig. 6 – Cross-sectional back scatter electron SEM images of the DCPNed sample (a) centre area (b) edge area.

Please cite this article in press as: Lin K, et al., Active screen plasma nitriding of 316 stainless steel for the application of bipolar plates in proton exchange membrane fuel cells, International Journal of Hydrogen Energy (2014), http://dx.doi.org/10.1016/j.ijhydene.2014.04.102

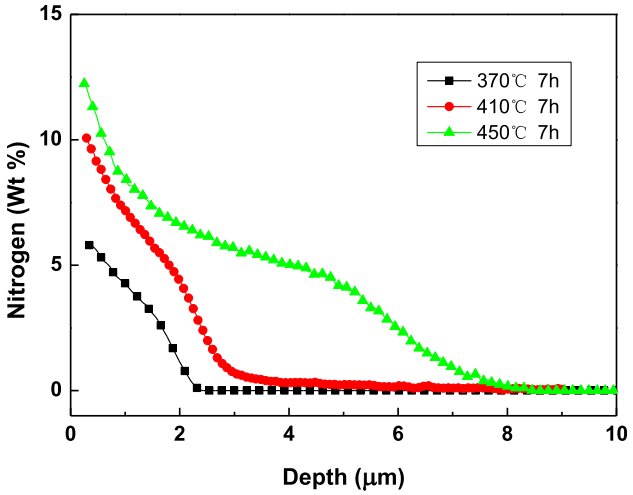

Fig. 7 – Concentration profile of nitrogen.

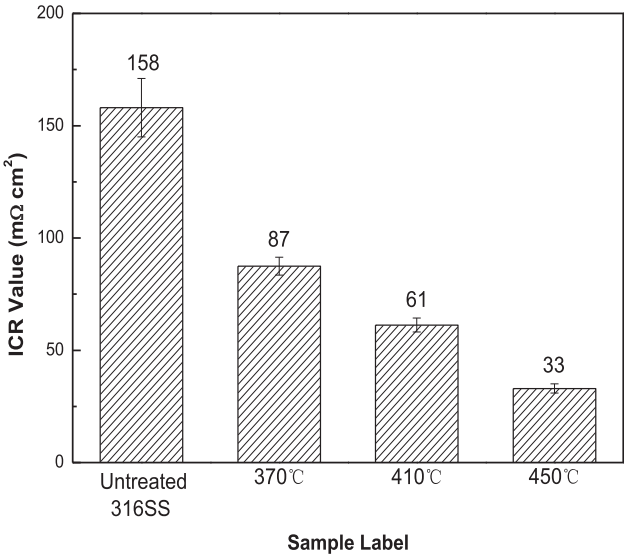

Fig. 9 – ICR value of untreated and ASP nitrided samples.

Interfacial contact resistance

The ICR values of the ASP nitrided samples were measured under the compaction force of 140 N/cm^2, which is the commonly applied force in fuel cell stacks. It has been reported that surface roughness has a significant influence on the ICR values measured [28]. Therefore, the ICR value of an untreated bare 316 stainless steel sample with a surface roughness of Ra = 0.120 μm, which was similar to the 450 °C treated sample (Ra = 0.115 μm) was also measured for comparison. Fig. 9 shows that the ICR value was reduced dramatically after all the ASPN treatments; the ICR values of the ASPN treated samples decreased with the increase of the treatment temperature. The ICR value of the 450 °C treated sample was the lowest, only one fifth of the untreated bare material. The ICR value of 450 °C DC plasma nitrided (DCPNed) samples was also measured for comparison and the results are shown in Fig. 10. When treated under similar conditions, the surface roughness of the DCPNed sample is higher than that of the ASP nitrided sample; but the ICR value of the DCPNed sample is marginally lower than that of the ASP nitrided sample. Therefore, taking the relatively higher surface roughness of the DCPNed sample into consideration, the surface conductivity of the DCPNed sample and the ASP nitrided samples treated under the same condition should be almost the same.

Some literatures report the enhancement of the surface conductivity of stainless steel after conventional low temperature plasma nitriding treatment [16,29,30], which is in agreement with the results of this work. Therefore, the nitrogen supersaturated phase, S-phase, possesses the capability of improving the surface conductivity of austenitic stainless steels.

Corrosion tests

Potentiodynamic corrosion tests were carried out to evaluate the corrosion resistance of untreated and ASP nitrided

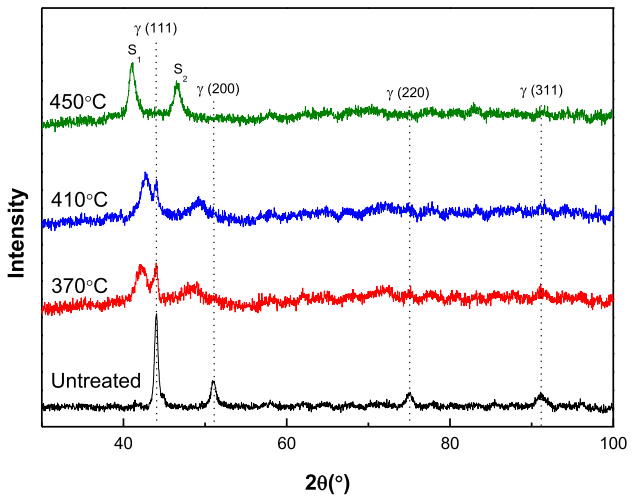

Fig. 8 – XRD patterns of samples before and after ASPN treatment.

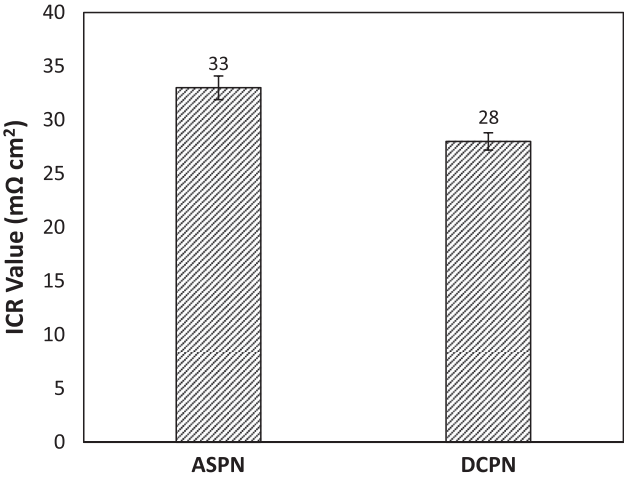

Fig. 10 – ICR value of ASPN and DCPN samples treated under 450 °C, 7 h and 4 mbar.

Please cite this article in press as: Lin K, et al., Active screen plasma nitriding of 316 stainless steel for the application of bipolar plates in proton exchange membrane fuel cells, International Journal of Hydrogen Energy (2014), http://dx.doi.org/10.1016/j.ijhydene.2014.04.102

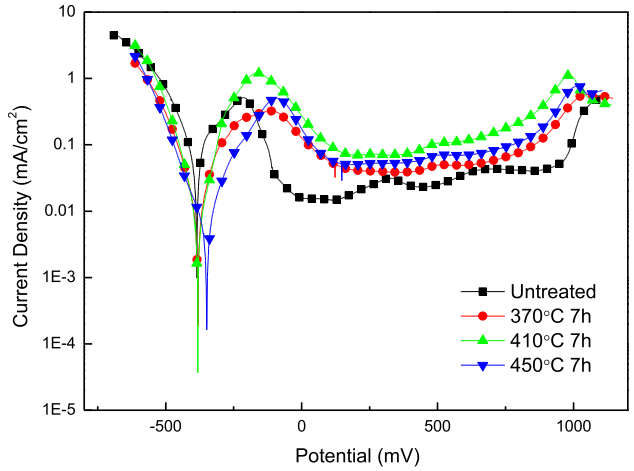

Fig. 11 – Polarization curves of bare and nitrided sample.

samples, and the polarization curves are given in Fig. 11. The trend of the curves of nitrided samples was similar with the untreated one, consisting of three stages, activation, passive and trans-passive. Based on the polarization curves, the corrosion potential (E_{corr}) and the corrosion current density (I_{corr}) were identified and Table 2 lists the corrosion potential (E_{corr}) and the corrosion current density (I_{corr}) of untreated and ASP nitrided samples. The corrosion potential of 370 and 410 °C nitrided sample was almost equal to that of the untreated one, but 450 °C nitrided sample had a slight more positive corrosion potential. From the corrosion current density point of view, all the nitrided samples exhibited better corrosion resistance than that of the untreated one, with the corrosion current density of the nitrided samples beings one order of magnitude lower than that of the untreated material. The corrosion tests of the 450 °C/7 h DCPN treated samples were also conducted, and the results are listed in Table 3. It can be seen that the corrosion resistance of 316 stainless steel degraded significantly by the DCPN treatment. It is noted from Fig. 11 that the passive current density of the nitrided samples is high than the untreated bare material, which will be discussed in the discussion section.

The surface morphology of untreated and nitrided samples after polarization tests were shown in Fig. 12. Although pits can be found from the nitrided samples after corrosion tests (Fig. 12(b)–(d)), the density of pits is much lower than that formed in untreated material (Fig. 12(a)), which is in agreement with the results of electrochemical tests. This indicates that the ASPN treatment has changed the dominating corrosion mechanism from localized corrosion to general

Table 2 – Corrosion potential and corrosion current density of bare and nitrided samples.

Sample	I_{corr}(mA/cm^2)	E_{corr} (mV)
Bare	0.0850	−386
370 °C	0.0098	−381
410 °C	0.0043	−382
450 °C	0.0063	−349

Table 3 – Corrosion potential and corrosion current density of ASPN and DCPN samples under 450 °C, 7 h and 4 mbar.

Sample	I_{corr} (mA/cm^2)	E_{corr} (mV)
ASPN	0.0063	−349
DCPN	0.0341	−401

corrosion. The mechanism involved in the improved corrosion resistance due to the introduction of N, has been extensively studied [21]. The widely accepted mechanism is that: nitrogen in nitrided layer would dissolve during corrosion process and consume the acid in pits, and thereby increases the pH value near the pits on the corrosion surface, leading to a relatively lower growth rate of pits. The nitrogen dissolution reaction may be represented as:

$$[N] + 4H^+ + 3e^- \rightarrow NH_4^+$$

Discussion

As reported above, compared with the untreated materials, the ASP nitrided samples possessed a remarkably reduced corrosion current density (I_{corr}) and slightly higher corrosion potential (E_{corr}). However, the passive current density for the nitrided samples is high than that for the untreated material. The relatively higher passive current density of the ASP nitrided sample could be related to the deposition layer on the top of the nitrided samples. The influence of the deposition layers on the corrosion resistance might be twofold. Firstly, due to the roughened surface (Figs. 3 and 4) the deposited layer would highly increase the real corroding area, and so the real passive current density should be lower than the apparent value. Secondly, these layers were sputtered from the screen, which is made of carbon steel. The corrosion resistance of carbon steel is much poorer than 316 stainless steel. In order to investigate the influence of screen materials on the corrosion resistance of ASP nitrided 316 stainless steel, ASPN treatments with carbon steel screen (CS) and 316 stainless steel screen (SS) were conducted at 450 °C for 7 h in a laboratory scale active screen set-up.

The surface morphologies of ASP nitrided samples with different screens are shown in Fig. 13. It can be clearly seen that, the size of deposited particles is much smaller when using the stainless steel screen (SS, 200 nm) than using the carbon steel screen (CS, 300 nm). In addition, the deposition layer formed using SS is denser, thus less pits, than that formed using CS, which might be less harmful for corrosion resistance. Although the surface morphology is slightly different when using different screens, their surface roughness and layer thickness are very similar, around 0.12 μm and 8 μm, respectively.

The surface EDS results of these two ASP nitrided samples with different screens are listed in Table 4. It can be seen that the amount of alloying elements in the SS sample is much higher than that in the CS sample. The absolute amount of the major alloying elements within the surface of the SS sample seems slightly lower than that in untreated 316 stainless steel. This is mainly due to the diluting effect of nitrogen introduced

Please cite this article in press as: Lin K, et al., Active screen plasma nitriding of 316 stainless steel for the application of bipolar plates in proton exchange membrane fuel cells, International Journal of Hydrogen Energy (2014), http://dx.doi.org/10.1016/j.ijhydene.2014.04.102

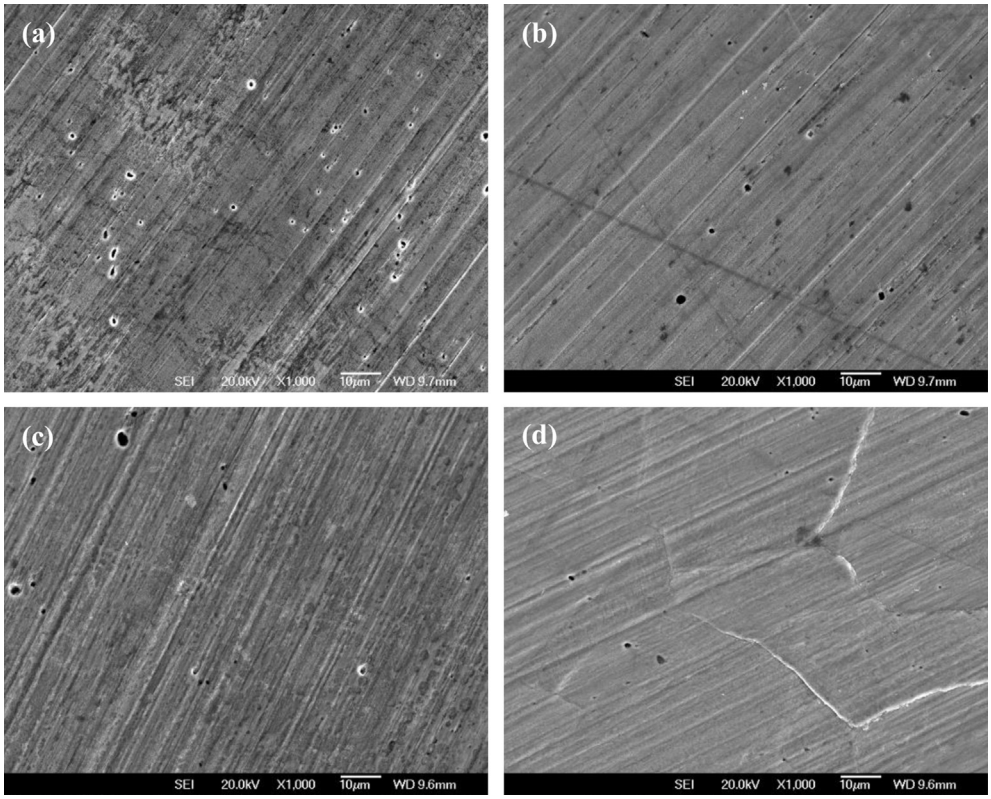

Fig. 12 – Surface morphology of corroded surface (a) untreated 316 stainless steel. (b) 370 °C 7 h (c) 410 °C 7 h (d) 450 °C 7 h.

by ASPN. It seems strange to find that the CS sample surface also contained a high amount of such alloying elements as Cr, Ni & Mo, which is typical for 316 austenitic stainless steel. This is most likely caused by the fact that the thickness of the deposition layer is much smaller than the penetration depth of electron beam.

From the XRD results shown in Fig. 14, differences in phase constituents between the CS and SS samples can be identified. Firstly, apart from the peaks of S-phase, the peaks of Fe_4N and Fe_3N were also detected from the CS sample. The presence of such iron nitrides could be explained by the mechanism of ASPN involving sputtering of iron from the steel screen, reaction of iron with nitrogen to form iron nitrides and deposition of the iron nitrides [31]. Secondly, the intensity of the S-phase peaks from the CS sample is greatly lower than that from the SS sample, which could be attributed to the formation of the iron nitrides on the surface of the CS sample.

The potentiodynamic polarization curves of the untreated and ASP nitrided samples using different screen materials were drawn in Fig. 15. The passive current densities of all samples are in the same order of magnitude; however, the passive current density of the ASP nitrided samples is slightly

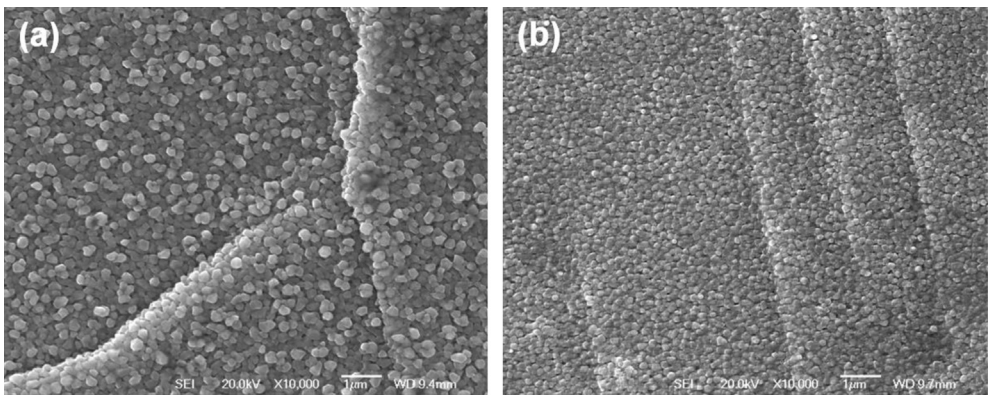

Fig. 13 – Surface morphology of active screen plasma nitrided samples with different screen material (a) Carbon steel screen. (b) Stainless steel screen.

Please cite this article in press as: Lin K, et al., Active screen plasma nitriding of 316 stainless steel for the application of bipolar plates in proton exchange membrane fuel cells, International Journal of Hydrogen Energy (2014), http://dx.doi.org/10.1016/j.ijhydene.2014.04.102

Table 4 – Surface EDS results of samples.

Sample label	Weight%							
	C	N	O	Cr	Mn	Fe	Ni	Mo
Bare 316 SS	3.20	–	0.11	16.89	1.54	65	10.88	2.37
CS	2.52	5.53	1.35	9.61	0.78	74.17	5.19	0.86
SS	2.87	5.23	1.74	14.04	1.46	62.78	10.1	1.78

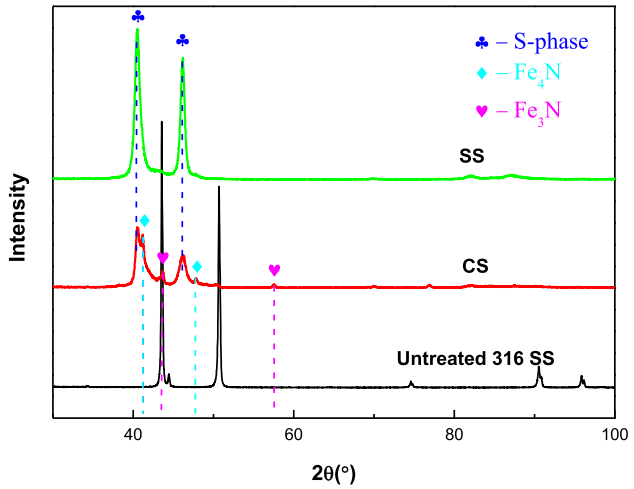

Fig. 14 – XRD results of different samples.

higher than that of the untreated material most probably due to increased surface roughness and hence the corroded surface areas.

It is of interest to note that in the potential range from −130 mV to 240 mV, the current density of the SS sample is lower than that of the CS sample, although the current densities are almost identical for the rest potential range. In addition, the corrosion current density is lower and the corrosion potential is more positive for the SS sample than for the CS sample (Table 5). Clearly, the SS sample possessed a better corrosion resistance than the CS sample. The relatively low density and the formation of iron nitrides may have contributed to the relatively poor corrosion resistance of the CS sample.

As reported in our previous paper [32], it is possible to alloy the surface of austenitic stainless steel with both interstitial elements (such as N and C) and substitutional elements (such as Ag and Cu) using a composite screen for active screen plasma treatment. Therefore, the corrosion resistance of the active screen plasma nitrided surface could be further improved by active screen plasma co-alloying with both C/N to form S-phase and noble elements to enhance corrosion properties, which will be reported in a further paper.

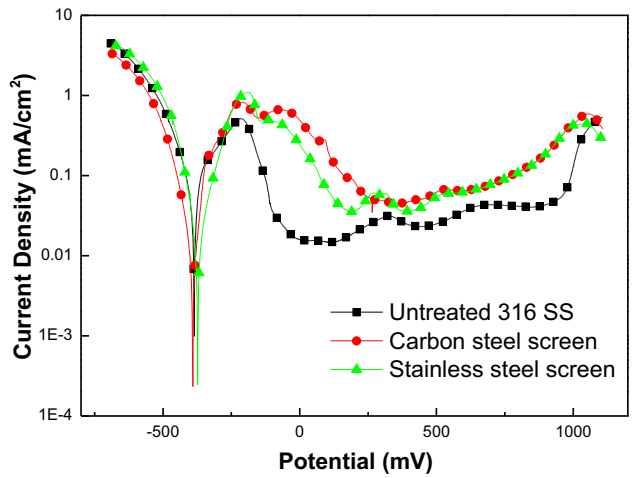

Fig. 15 – The potentiodynamic polarization curves of different treated samples.

Conclusions

In this work, the feasibility of improving the surface properties of AISI316 austenitic stainless steel by advanced active screen plasma (ASP) nitriding has been studied. Based on the experimental results and discussion, the following conclusions can be drawn:

- Nitrogen supersaturated S-phase layers have been successfully produced on the surface of 316 austenitic stainless steel using low-temperature (370–450 °C) active screen plasma nitriding.
- The active screen plasma nitriding can significantly reduce the interfacial contact resistance (ICR) value of 316 austenitic stainless steel mainly due to the formation nitrogen supersaturated S-phase layer; the ICR value of the nitrided samples decreased with increasing the treatment temperature.
- The electrochemical corrosion resistance of 316 steel in 0.05 M H_2SO_4 solution can be improved by low-temperature active screen plasma nitriding in terms of reduced corrosion current density and increased corrosion potential.
- The passive current density of the ASP nitrided 316 steel is slightly higher than that for the untreated material largely due to the deposited surface iron nitride particles and hence the increased corroding areas.
- Due to the inherent edge effect associated with conventional DC plasma nitriding, the corrosion resistance of the DC plasma nitrided 316 is inferior to that of active screen plasma nitrided one.

Table 5 – Results of corrosion tests.

Sample	I_{corr}(mA/cm^2)	E_{corr} (mV)
Bare 316 stainless steel	0.085	−386
Carbon steel screen	0.080	−391
Stainless steel screen	0.018	−373

Please cite this article in press as: Lin K, et al., Active screen plasma nitriding of 316 stainless steel for the application of bipolar plates in proton exchange membrane fuel cells, International Journal of Hydrogen Energy (2014), http://dx.doi.org/10.1016/j.ijhydene.2014.04.102

- The corrosion resistance of active screen plasma nitrided 316 steel also depends on the material of the active screen with stainless steel screen offering a better corrosion resistance over carbon steel screen.

Therefore, low-temperature active screen plasma nitriding is a promising method to modify the surface of 316 stainless steel for bipolar plate application.

Acknowledgements

The authors would like thank Engineering and Physical Sciences Research Council, UK(EP/J018252) for the financial support to the research. The School of Metallurgy and Materials, the University of Birmingham and the China Scholarship Council (CSC) are also acknowledged for providing PhD scholarship for Kaijie Lin.

REFERENCES

[1] Tsuchiya H, Kobayashi O. Mass production cost of PEM fuel cell by learning curve. Int J Hydrogen Energy 2004;29:985–90.
[2] Hermann A, Chaudhuri T, Spagnol P. Bipolar plates for PEM fuel cells: a review. Int J Hydrogen Energy 2005;30:1297–302.
[3] Lee SJ, Huang CH, Lai JJ, Chen YP. Corrosion-resistant component for PEM fuel cells. J Power Sources 2004;131:162–8.
[4] Tawfik H, Hung Y, Mahajan D. Metal bipolar plates for PEM fuel cell – a review. J Power Sources 2007;163:755–67.
[5] Ren YJ, Chen J, Zeng CL. Corrosion protection of type 304 stainless steel bipolar plates of proton-exchange membrane fuel cells by doped polyaniline coating. J Power Sources 2010;195:1914–9.
[6] Tian RJ, Sun JC. Corrosion resistance and interfacial contact resistance of TiN coated 316L bipolar plates for proton exchange membrane fuel cell. Int J Hydrogen Energy 2011;36:6788–94.
[7] Fu Y, Hou M, Xu HF, Hou ZJ, Ming PW, Shao ZG, et al. Ag-polytetrafluoroethylene composite coating on stainless steel as bipolar plate of proton exchange membrane fuel cell. J Power Sources 2008;182:580–4.
[8] Yun YH. Deposition of gold-titanium and gold-nickel coatings on electropolished 316L stainless steel bipolar plates for proton exchange membrane fuel cells. Int J Hydrogen Energy 2010;35:1713–8.
[9] Wang H, Brady MP, Teeter G, Turner JA. Thermally nitrided stainless steels for polymer electrolyte membrane fuel cell bipolar plates – part 1: model Ni-50Cr and austenitic 349 (TM) alloys. J Power Sources 2004;138:86–93.
[10] Wang H, Brady MP, More KL, Meyer HM, Turner JA. Thermally nitrided stainless steels for polymer electrolyte membrane fuel cell bipolar plates – part 2: beneficial modification of passive layer on AISI446. J Power Sources 2004;138:79–85.
[11] Lee SH, Kim JH, Lee YY, Wee DM. Effects of low-temperature nitridation on the electrical conductivity and corrosion resistance of 446M stainless steel as bipolar plates for proton exchange membrane fuel cell. Int J Hydrogen Energy 2010;35:725–30.
[12] Dong H. S-phase surface engineering of Fe–Cr, Co–Cr and Ni–Cr alloys. Int Mater Rev 2010;55:65–98.
[13] Zhang ZL, Bell T. Structure and corrosion resistance of plasma nitrided stainless steel. Surf Eng 1985;1:131–6.
[14] Tian RJ, Sun JC, Wang JL. Study on behavior of plasma nitrided 316L in PEMFC working conditions. Int J Hydrogen Energy 2008;33:7507–12.
[15] Tian RJ, Sun JC, Wang L. Effect of plasma nitriding on behavior of austenitic stainless steel 304L bipolar plate in proton exchange membrane fuel cell. J Power Sources 2007;163:719–24.
[16] Hong W, Han DH, Choi H, Kim MW, Lee JJ. High-density plasma nitriding of AISI 316L for bipolar plate in proton exchange membrane fuel cell. Int J Hydrogen Energy 2011;36:2207–12.
[17] Kaestner P, Michler T, Weidner H, Rie KT, Brauer G. Plasma nitrided austenitic stainless steels for automotive hydrogen applications. Surf Coat Technol 2008;203:897–900.
[18] Gallo SC, Dong H. Corrosion behaviour of direct current and active screen plasma carburised AISI 316 stainless steel in boiling sulphuric acid solutions. Corros Eng Sci Technol 2011;46:8–16.
[19] Georges IJ, Cleugh D. Active screen plasma nitriding in stainless steel. Thermochem Surf Eng Stainl Steel; 2000:377–87.
[20] Li CX, Georges J, Li XY. Active screen plasma nitriding of austenitic stainless steel. Surf Eng 2002;18:453–8.
[21] Li CX, Bell T. Corrosion properties of active screen plasma nitrided 316 austenitic stainless steel. Corros Sci 2004;46:1527–47.
[22] Gallo SC, Dong HS. On the fundamental mechanisms of active screen plasma nitriding. Vacuum 2009;84:321–5.
[23] Li CX. Active screen plasma nitriding – an overview. Surf Eng 2010;26:135–41.
[24] Sun Y. Depth-profiling electrochemical measurements of low temperature plasma carburised 316L stainless steel in 1 M H_2SO_4 solution. Surf Coat Technol 2010;204:2789–96.
[25] Wang HL, Sweikart MA, Turner JA. Stainless steel as bipolar plate material for polymer electrolyte membrane fuel cells. J Power Sources 2003;115:243–51.
[26] Li CX, Bell T, Dong H. A study of active screen plasma nitriding. Surf Eng 2002;18:174–81.
[27] Ichii K, Fujimura K, Takase T. Structure of the ion-nitrided layer of 18-8 stainless steel. Technol Rep Kansai Univ 1986;27:135–44.
[28] Kraytsberg A, Auinat A, Ein-Eli Y. Reduced contact resistance of PEM fuel cell's bipolar plates via surface texturing. J Power Sources 2007;164:697–703.
[29] Tian RJ, Sun JC, Wang L. Plasma-nitrided austenitic stainless steel 316L as bipolar plate for PEMFC. Int J Hydrogen Energy 2006;31:1874–8.
[30] Flis J, Kuczynska M. Effect of low-temperature plasma nitriding on corrosion of 304L stainless steel in sulfate and chloride solutions. J Electrochem Soc 2004;151:B573–80.
[31] Zhao C, Li CX, Dong H, Bell T. Study on the active screen plasma nitriding and its nitriding mechanism. Surf Coat Technol 2006;201:2320–5.
[32] Dong Y, Li X, Tian L, Bell T, Sammons RL, Dong H. Towards long-lasting antibacterial stainless steel surfaces by combining double glow plasma silvering with active screen plasma nitriding. Acta Biomater 2011;7:447–57.

Please cite this article in press as: Lin K, et al., Active screen plasma nitriding of 316 stainless steel for the application of bipolar plates in proton exchange membrane fuel cells, International Journal of Hydrogen Energy (2014), http://dx.doi.org/10.1016/j.ijhydene.2014.04.102